

www.chemeurj.org

An Alternate [2×2] Grid Constructed Around TiO₄N₂ Units

Erin Day,^[a] Brice Kauffmann,^[b] Matthieu Scarpi-Luttenauer,^[a] Alain Chaumont,^[c] Marc Henry,^[a] and Pierre Mobian*^[a]

Abstract: The formation of a tetranuclear self-assembled species constructed around a TiO_4N_2 motif is reported. This aggregate is generated from $Ti(O^iPr)_{4'}$ 2,2'-bipyrimidine (bpym) and a bis-biphenol strand (L^2H_4) where two 2,2'-biphenol units are connected with a biphenyl spacer. The solid-state structure of the $[Ti_4(L^2)_4(bpym)_4]$ architecture reveals the formation of an unprecedented chiral alternate $[2\times2]$ grid. In addition to the structural characterization of the $[Ti_4(L^2)_4(bpym)_4]$ architecture, geometry optimisation on various possible isomeric tetrameric assemblies ($[2\times2]$ grid, alternate $[2\times2]$ grid, circular helicate or cyclic hemihelicate) is

performed using DFT calculations. These results confirm the higher stability of the alternate $[2\times2]$ grid over the other possible tetranuclear isomers and allow examining the replacement of the bpym ligands by two novel diimine chelates within the tetranuclear assembly (2,2'-bipyridine=bipy and 2,2'-bipyrazine=bipyraz). From this initial theoretical investigation, the competition between these three nitrogen ligands in the course of the self-assembly process is next evaluated. Overall, this investigation shows that the exclusive formation of the alternate $[2\times2]$ grid is driven by CH···N interactions.

Introduction

Self-assembly driven by coordination bonds is a highly powerful approach to generate giant complex architectures^[1] and functional arrays^[2] from rather simple building blocks. Thus, an impressive variety of self-assembled metallo-architectures have been reported including linear and circular helicates, [3,4] topological non-trivial molecules, [5-7] metallo-squares, [8] cages or giant spheres. [9-13] Metallosupramolecular grids[14-16] are a particular class of self-assembled architectures that have attracted major interest due to their redox, magnetic or spin-state transition properties.[17-25] The construction of such metal ion arrays is based on the mutual recognition of directional ligands (L) and metal ions (M) leading to an orthogonal arrangement of the ligands at each metal corner. The $[2\times2]$ grids (Figure 1) are archetypes of this family of molecules. [26,27] These tetranuclear ion arrays are obtained by reacting a ligand possessing two coordination subunits with a metal ion having generally a tetrahedral, bipyramidal or an octahedral geometry. [28][29] Nevertheless, depending on the flexibility of the ligand, isomeric M₄L₄ architectures can be obtained as circular helicate, alternate [$2\times$

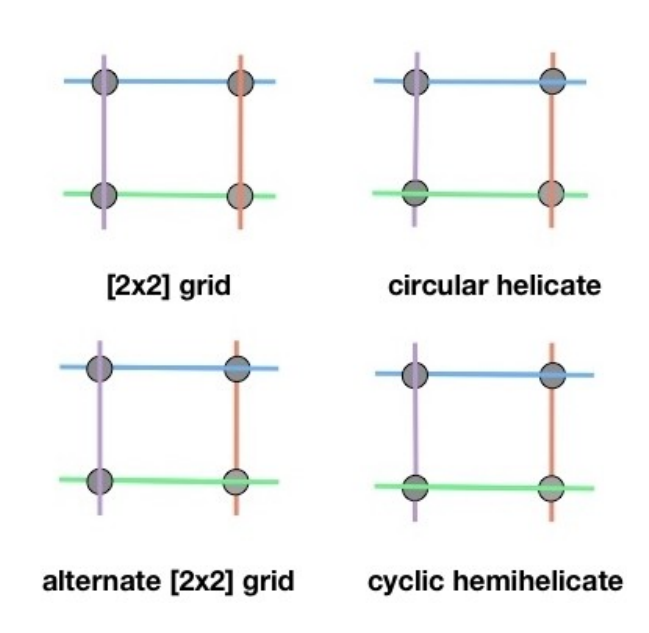


Figure 1. Schematic representation of a [2 \times 2] grid and three isomeric M_4L_4 cyclic structures.

2] grid or cyclic hemihelicate. Four possible isomers are schematically represented in Figure 1. Whereas cyclic tetranuclear helicates and $[2\times2]$ grids are rather common species, the two closely related architectures (the cyclic hemihelicate and the alternate $[2\times2]$ grid) are exceptions and are considered as synthetic curiosities. Also, note that the cyclic helicates or hemihelicates are intrinsically chiral architectures, whereas the grid-type assemblies are achiral assemblies.

In the field of metallosupramolecular architectures, Ti(IV) ions are extensively used to construct assemblies and a large number of dinuclear helicate-like Ti(IV) complexes have been reported with organic strands including phenol-based or

[[]a] E. Day, M. Scarpi-Luttenauer, M. Henry, P. Mobian Laboratoire de Chimie Moléculaire de l'Etat Solide UMR 7140 UDS-CNRS, Université de Strasbourg 4 rue Blaise Pascal, 67000 Strasbourg (France) E-mail: mobian⊚unistra.fr

[[]b] B. Kauffmann Univ. Bordeaux, IECB, UMS 3033/US 001 2 rue Robert Escarpit, 33607 Pessac (France)

[[]c] A. Chaumont

Laboratoire de Modélisation et Simulations Moléculaires

UMR 7140 UDS-CNRS, Université de Strasbourg

4 rue Blaise Pascal, 67000 Strasbourg (France)

Supporting information for this article is available on the WWW under https://doi.org/10.1002/chem.202200047



benzene-o-dithiol ligands. [33-35] Recently, Albrecht and coworkers [36] or Yashima and co-workers [37] have elegantly demonstrated that dinuclear Ti(IV) helicates are highly promising to develop new types of molecular devices. Also, the construction of trinuclear titanium self-assembled complexes has been largely tackled. [38,39] By comparison with dinuclear or trinuclear species, discrete Ti(IV)-assemblies with higher nuclearities are less accessible. Ti(IV)-based cages [40] or cubes [41] are representative examples of these self-assembled species including more than three metallic centres.

In our effort to generate multicomponent self-assembled polynuclear architectures built up around TiO₄N₂ centres, we have extensively employed a bis-biphenol pro-ligand (L1H4) where the two biphenol units are connected through a pphenylene spacer (Figure 2).[42] This pro-ligand has proved to be ideally designed to afford several neutral helicate systems with Ti(OⁱPr)₄ and nitrogen ligands. Dinuclear Ti(IV)-based doublestranded helicates were obtained with monodentate^[43] or bidentate nitrogen ligands.[44,45] Also, we have shown that the nuclearity of these architectures formed around TiO₄N₂ units is tuned by the choice of the bidentate nitrogen ligand as a bowlshaped circular trinuclear helicate could be isolated by applying a multicomponent self-assembly reaction with the 2,2'-bipyrchelate^[46] imidine (bpym) or bis((anthryl)vinyl)2,2'bipyrimidine.[47] Herein, we examine how a structural modification of the bis-biphenol could impact the structure and/or the nuclearity of the final aggregate. Thus, we report in this article the self-assembly of a novel bis-biphenol strand (L²H₄, Figure 2) with Ti(OiPr)₄ and bpym. L²H₄ differs from L¹H₄ only by the spacer linking the two biphenol units since L²H₄ includes a biphenyl spacer. The first part of this article details the synthesis of this fully aromatic oligophenol strand and the full characterization including single-crystal X-ray diffraction (SC-XRD) analysis of the final self-assembled alternate $[2\times2]$ grid obtained with this tetrahydroxyoligophenylene proligand, Ti(OⁱPr)₄ and bpym, Next, using DFT calculations we investigate the energy associated with the alternate $[2\times2]$ grid isomer versus those determined for the other tetrameric isomers i.e. the $[2\times2]$ grid, the circular helicate or the cyclic hemihelicate (Figure 1). This allowed to retrieve the factors explaining the selectivity of the

OH

$$n = 0: L^1H_4$$
 $n = 1: L^2H_4$
 $X = N, Y = CH: bipym$
 $X = CH, Y = CH: bipy$
 $X = CH, Y = CH: bipy$
 $X = CH, Y = CH: bipy$

Figure 2. Ligands discussed in this article.

self-assembly process and subsequently to understand the results gained from a selection study.

Results and Discussion

Synthesis of L²H₄ and [Ti₄(L²)₄(bpym)₄]

The synthetic strategy of L^2H_4 was inspired from the one used to afford L^1H_4 . [42] L^2H_4 was obtained in two steps starting from the 2,2'-dimethoxy-[1,1':3',1"-terphenyl]-3-yl-boronic acid (see Figure 3). This boronic acid was engaged in a Suzuki-Miyaura cross-coupling reaction with 4,4'-dibromo-1,1'-biphenyl to give in a 67% yield the methylated analogue of L^2H_4 . The methoxy groups were cleaved with BBr₃ to produce the targeted compound in an excellent yield (90%).

Next, the multicomponent self-assembly reaction was tested in an equimolar ratio of $L^2H_4/Ti(O^iPr)_4/bpym$ as described in Equation (1):

$$4 L^{2}H_{4} + 4 Ti(O^{i}Pr)_{4} + 4 bpym$$

 $\rightarrow [Ti_{4}(L^{2})_{4}(bpym)_{4}] + 16 HO^{i}Pr$ (1)

The reaction was performed in chloroform under solvothermal conditions at 100 °C. After one week, red crystals appeared in the medium. These crystals were isolated with a yield of 81%. The ES-MS analysis of the crystals displays only a weak peak at high m/z (see Figure 4). The simulated isotopic profile of a doubly charged species formulated as $[{\rm Ti_4(L^2)_4(bpym)_4} + {\rm 2H}]^{2+}$ matches with the experimental isotopic profile at m/z=1753.45.

The diffusion ordered spectroscopy (DOSY) analysis of a CD_2Cl_2 solution obtained by dissolving the red crystals proved the presence of a sizeable species. The diffusion was measured $(D=430\pm10\,\%\,\mu\text{m}^2.\text{s}^{-1})$, significantly lower than the diffusion previously reported for a double-stranded helicate formed with

Figure 3. Synthetic route leading to the L²H₄ strand.

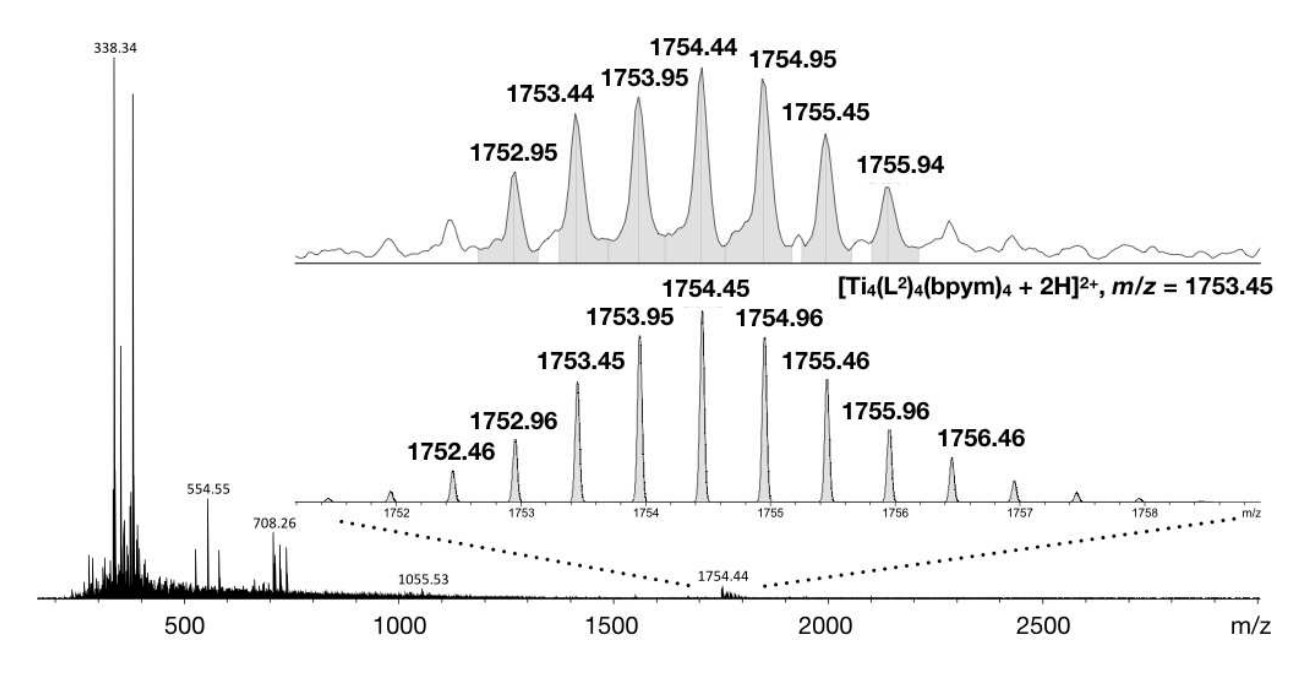


Figure 4. ES-MS spectrum of the isolated crystals attesting the formation of a tetranuclear species. Enlargement of the peak at m/z = 1753.44 with the isotopic simulation (enlargement bottom) corresponding a complex formulated as $[Ti_4(L^2)_4(bpym)_4]$ (calcd for $[Ti_4(L^2)_4(bpym)_4 + 2H]^{2+}$, m/z = 1753.45).

L¹ constructed around two TiO_4N_2 units $(D=600\pm10\,\%\,\mu\text{m}^2.\text{s}^{-1})$, [44] confirming the presence in solution of a large compound. According to the Stokes-Einstein equation, the diffusion corresponds to a species having a hydrodynamic radius large enough to account for the tetranuclear structure $(R_h=11.1\pm1.1~\text{Å})$. Next, the solution was analysed by ¹H NMR. Due to the various overlapping signals of the spectrum spread from 10 ppm to 6 ppm, each signal could not be accurately assigned (see Figure 5). However, in this aromatic region several signals could be distinguished that correspond to the more downfield resonances of the deshielded 2,2′ protons and the 4,4′ protons belonging to the bpym chelates. A total of eight doublets of doublet, integrating for two protons each, $(\delta=9.88, 8.95, 8.84, 8.74, 8.33, 8.26, 7.95$ and 7.93 ppm) are counted (see

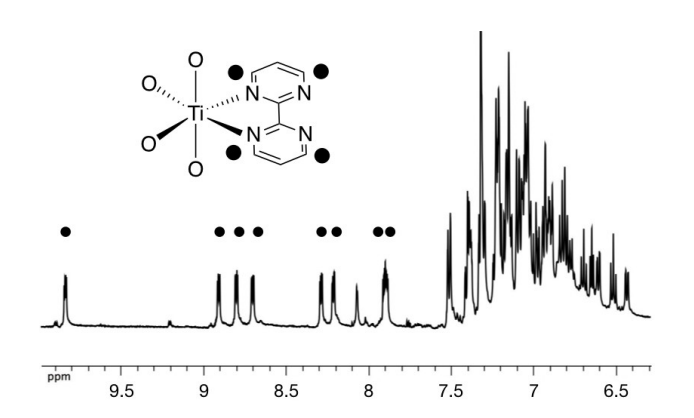


Figure 5. Aromatic region of the ¹H NMR spectra of $[\mathrm{Ti}_4(\mathrm{L}^2)_4(\mathrm{bpym})_4]$ (CD₂Cl₂, 500 MHz). The signals marked with the round black spots are assigned to the resonances of the 2,2' protons and the 4,4' protons belonging to the bpym chelate within $[\mathrm{Ti}_4(\mathrm{L}^2)_4(\mathrm{bpym})_4]$, reflecting a C_2 -symmetry for the complex.

Figure 5). This ¹H NMR signature highlights the symmetry of the $[Ti_4(L^2)_4(bpym)_4]$ complex and indicates that the assembly incorporated two nonequivalent pairs of bipyrimidine chelates. Altogether, these data unambiguously indicate that the $[Ti_4(L^2)_4(bpym)_4]$ assembly possesses a C_2 symmetry in solution.

The crystal structure of the complex obtained by X-ray diffraction is given in Figure 6. This structure confirms the formation of a nanosized architecture having the [Ti₄(L²)₄(bpym)₄] formula and corresponding to an aggregate of 48 molecules. The compound crystallizes in a giant orthorhombic unit cell containing three molecules in the asymmetric unit (a = 50.5331(8) Å, b = 121.3748(15) Å and c = 41.8102(8) Å).Among the possible M₄L₄ cyclic isomers (Figure 1), this assembly displays the framework of an alternate [2×2] grid. However, $[Ti_4(L^2)_4(bpym)_4]$ is less symmetrical than a classical alternate $[2 \times$ 2] grid since the crystal structure highlights only a pseudo C_2 symmetry. In the crystal, [Ti₄(L²)₄(bpym)₄] does not adopt a perfect C2-symmetry as evidenced by the intermetallic distances (d(Ti–Ti) = 12.266 Å, 11.663 Å, 10.558 Å and 10.556 Å for one selected molecule). Also, we notice that these intermetallic distances within [Ti₄(L²)₄(bpym)₄] are rather high compared to previously reported metallogrid systems.[48] The pseudo C2symmetry determined in the solid-state for [Ti₄(L²)₄(bpym)₄] matches with the ¹H NMR signature for the complex in solution discussed above proving that the structure of [Ti₄(L²)₄(bpym)₄] characterized in the solid-state remained unaltered when the complex is dissolved in solution. The angles measured within the TiO₄N₂ coordination sphere as well as the Ti-O and Ti-N distances are comparable with those determined for other TiO₄N₂ architectures constructed with similar ligand systems (see Supporting Information). [Ti₄(L²)₄(bpym)₄] is a chiral molecule composed by four chiral vertices. The unit cell

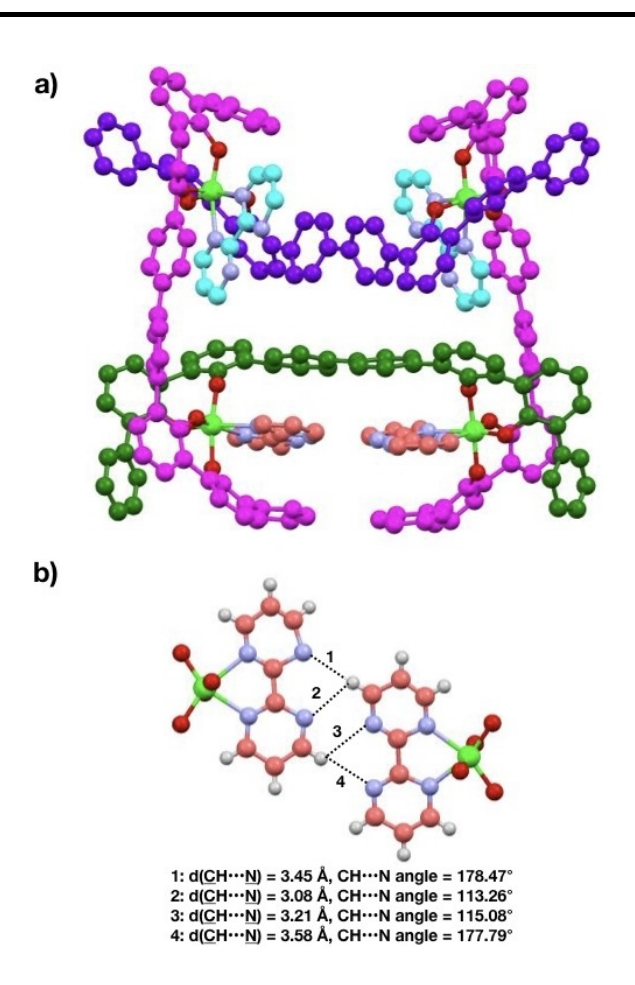


Figure 6. a) Ball and stick representation of the solid-state structure of $[\mathrm{Ti}_4(L^2)_4(\mathrm{bpym})_4]$ obtained from single-crystal X-ray crystallography. Hydrogen atoms are omitted for clarity. Titanium atoms are in light green. The ligands with a pseudo C_2 -symmetry relationship within the complex possess the same color code. b) The two coordinated bpym ligands in close contact within the $[\mathrm{Ti}_4(L^2)_4(\mathrm{bpym})_4]$. The dotted lines symbolise the intramolecular N···HC interactions between two bpym ligands.

contains the $(\Lambda,\Lambda,\Lambda,\Lambda)$ - $[Ti_4(L^2)_4(bpym)_4]$ and $(\Lambda,\Delta,\Lambda,\Lambda)$ - $[Ti_4(L^2)_4(bpym)_4]$ enantiomers. We note, at two Ti nodes within $[Ti_4(L^2)_4(bpym)_4]$, that the two bpym ligands orient themselves toward one another, owing to the hydrogen bond interactions between CH···N. Figure 6b emphasizes these intramolecular CH···N short distances for one selected complex $(d(\underline{C}H \cdot \cdot \cdot \underline{N}) = 3.45 \text{ Å}, 3.08 \text{ Å}, 3.21 \text{ Å} and 3.58 \text{ Å})$ between two neighbouring coordinated bpym ligands. Thus, from the solid-state structure, it is envisioned that these intramolecular interactions linked to the spatial disposition of the two neighbouring bpym ligands drive the formation of this alternate [2×2] grid structure.

DFT calculations

As it was established just above, the self-assembly process involving L^2H_4 , $Ti(O^iPr)_4$ and bpym leads only to the formation of the alternate [2×2] grid structure. However, the three additional isomeric architectures mentioned in the introduction could also be envisaged when the synthesis of tetrameric arrays

are tackled. At first glance, the synthesis of the alternate $[2 \times 2]$ grid was unexpected since [2×2] grids or circular tetranuclear helicates dominate the field of metallo-architectures composed of tetranuclear ion arrays. Therefore, it is a fundamental task to apprehend the factors driving the formation of the alternate $[2\times2]$ grid to the detriment of the $[2\times2]$ grid, the circular helicate or the cyclic hemihelicate. Thus, we investigated the relative stability of these four isomeric architectures via DFT calculations. Geometry optimizations in the gas phase of the four [Ti₄(L²)₄(bpym)₄] isomers were performed using the B3LYP functional and a LANL2DZ basis set. [49-51] Dispersion correction were added using Grimme's GD3 empirical correction. [52] We also tested the wB97XD functional^[53] and a LANL2DZ basis set. Results are given in Table S3 and follow the same trends as those obtained via the B3LYP functional. We will only further discuss results obtained via the latter functional. The previously obtained crystal structure served as starting point for geometry optimisation of the alternate $[2 \times 2]$ grid, the starting structures for the remaining isomers were derived from the former by modifying the structure by hand. For the circular helicate we considered two different initial configurations, namely a homochiral $\Delta\Delta\Delta\Delta$ and the heterochiral $\Delta\Delta\Delta\Lambda$. For the [2×2] grid as well as for the cyclic hemihelicate we also considered different initial configurations, however only the $\Lambda\Delta\Lambda\Delta$ configuration in the case of the former and the $\Delta\Delta\Lambda\Delta$ configuration in the case of the latter revealed to be initially sufficiently uncrowded to converge to an optimised geometry of the investigated complex. The resulting computed structures are given in Figure 7. The values determined for each [Ti₄(L²)₄(bpym)₄] cyclic architecture are compiled in Table 1.

Among these computed models of $[\mathrm{Ti_4(L^2)_4(bpym)_4}]$, it appears that the alternate $[2\times2]$ grid is undoubtedly the most stable architecture whereas the $[2\times2]$ grid is the less energetically favoured complex. Interestingly, the $[2\times2]$ grid model (Figure 8b) is the sole computed structure where the specific offset disposition of two bipyrimidine ligands facing each other as highlighted in the crystal structure of $[\mathrm{Ti_4(L^2)_4(bpym)_4}]$ (Figure 6b) is not found. This underlines the potential crucial

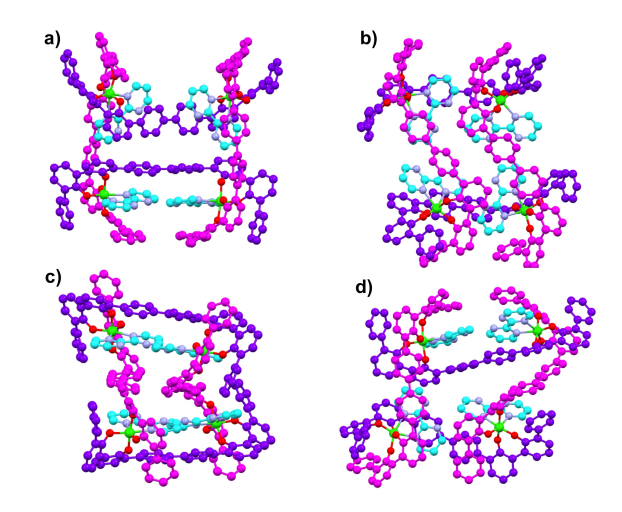


Figure 7. Modelled $[Ti_4(L^2)_4(bpym)_4]$ isomers: a) alternate $[2\times2]$ grid, b) $[2\times2]$ grid, c) homochiral cyclic helicate and d) cyclic hemihelicate.



Table 1. Absolute energy (in Hartree) as well as the relative energy (kJ/mol) of five isomeric $[Ti_4(L^2)_4(bpym)_4]$ cyclic structures obtained via DFT (B3LYP//LAN2DZ) calculations.

	Energy (Hartree)	$\Delta E_{\rm rel}$ [kJ/mol]
[Ti ₄ (L ²) ₄ (bpym) ₄]		
Alternate [2×2] grid	-10934.8935182	0.0
Cyclic hemihelicate	-10934.8740834	51.0
$\Delta\Delta\Delta\Lambda$ -Circular helicate	-10934.8664176	71.2
$\Delta\Delta\Delta\Delta$ -Circular helicate	-10934.8815146	7.5
[2×2] grid	-10934.8446350	128.3

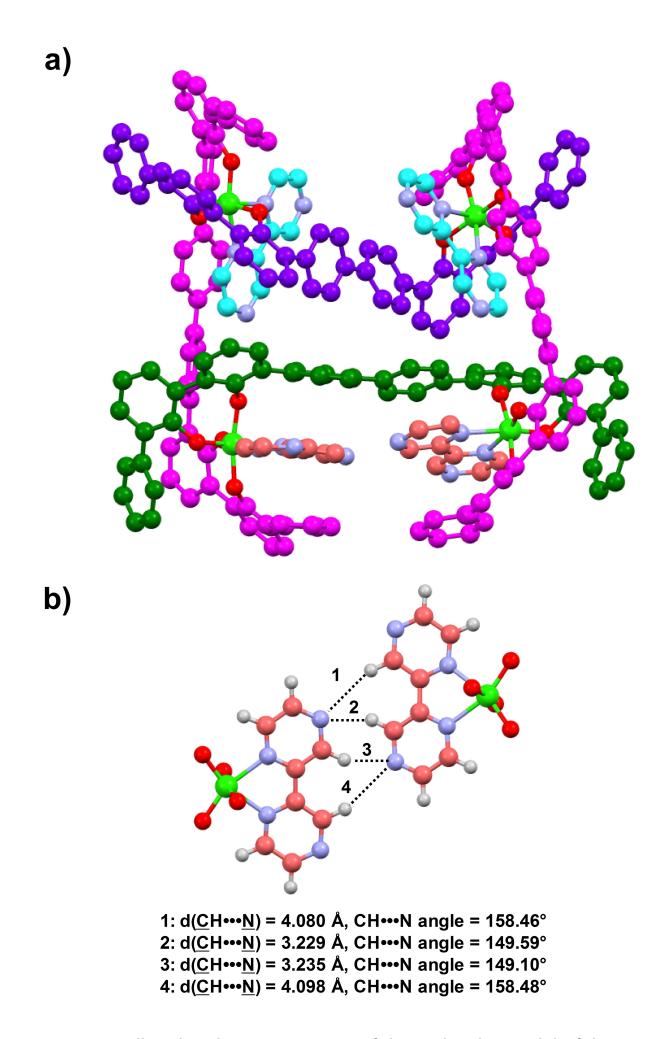


Figure 8. a) Ball and stick representation of the molecular model of the $[\mathrm{Ti}_4(\mathrm{L}^2)_4(\mathrm{bipyraz})_4]$ alternate grid obtained via DFT (B3LYP//LAN2DZ) calculations. Hydrogen atoms are omitted for clarity. Titanium atoms are in light green. The ligands with a pseudo C_2 -symmetry relationship within the complex possess the same color code. b) The two coordinated bipyraz ligands in close contact within the $[\mathrm{Ti}_4(\mathrm{L}^2)_4(\mathrm{bipyraz})_4]$ alternate $[2\times2]$ grid model. The dotted lines symbolise the intramolecular N···HC interactions between two bpym ligands.

role of intramolecular interactions (CH···N interactions) generated from the unique disposition of two neighbouring bpym ligands within the complex to stabilise these architectures. Additionally, the influence of a modification of the chirality at one metal centre on the overall energy of the circular helicate has been examined. Therefore, a new circular helicate model was computed starting from the initial $\Delta\Delta\Delta\Delta$ homochiral

circular helicate. This heterochiral architecture contains metallovertices displaying the following stereochemical descriptors: $\Delta,$ $\Delta,$ Δ and $\Lambda.$ The model is given in Supporting Information and a ΔE value of 63.7 kJ/mol in favor of the homochiral stereoisomer (see Table 1) is obtained showing that homochirality for the modelled circular helicate conducts to a more stable structure. It should be noted that the heterochiral computed model where the $\Delta,$ $\Delta,$ Λ and Λ configuration sequence is imposed for the metallo-vertices converges into an assembly for which the circular helicity is lost (see Supporting Information).

In order to inspect if these weak CH···N interactions are essential stabilizing factors for the alternate [2×2] grid, we constructed theoretical tetranuclear cyclic architectures where the 2,2'-bipyrimidine chelate were replaced by closely related diimine ligands. The 2,2'-bipyridine (bipy) and the 2,2'-bipyrazine (bipyraz) were selected. Indeed, for the structures constructed with bipy, no intramolecular CH···N interactions are possible. The modelled structures containing the bipyrazine ligands are built to evaluate the influence of the nitrogen atom positions onto these CH···N interactions. Geometry optimization of a given architecture with either 2,2'-bipyridine or 2,2'bipyrazine as ligand was started from the optimized structures obtained for the [Ti₄(L²)₄(bpym)₄] and modifying the nature of the ligand. The energies of the four tetranuclear isomers of $[Ti_4(L^2)_4(bipy)_4]$ and $[Ti_4(L^2)_4(bipyraz)_4]$ are given in Table 2. Similar trends have been found in the case of the bipy and bipyraz based structures as those observed for the $[Ti_4(L^2)_4(bpym)_4]$. It is however noteworthy to see that in the case of the 2,2'-bipyridine structures, the energy difference between the alternate $[2\times2]$ grid and the [2x2] grid is highly reduced (by about 80 kJ/mol) compared to the energy differences observed for the bipyrimidine and bipyrazine structures, pointing again to the importance of CH···N interactions in the latter two compounds. The modelled structure of the alternate [2×2] grid isomer of [Ti₄(L²)₄(bipyraz)₄] represented in Figure 8 contains key information. This computed structure highlights as observed for the alternate $[2\times2]$ grid $[Ti_4(L^2)_4(bpym)_4]$ complex, close contacts between two neighbouring coordinated bipyraz ligands as shown the enlargement of Figure 8b. Thus, the model of the alternate $[2\times2]$ grid $[Ti_4(L^2)_4(bipyraz)_4]$ complex attests similar CH···N interactions as those highlighted by the inspection of the crystal structure of the alternate $[2\times2]$

Table 2. Absolute energy (in Hartree) as well as the relative energy (kJ/mol) of the isomeric cyclic structures of $[Ti_4(L^2)_4(bipy)_4]$ and $[Ti_4(L^2)_4(bipyraz)_4]$ obtained via DFT (B3LYP // LAN2DZ) calculations.

	Energy (Hartree)	$\Delta E_{\rm rel}$ [kJ/mo])
[Ti ₄ (L ²) ₄ (bipy) ₄]		
Alternate [2×2] grid	-10806.7178520	0.0
Cyclic hemihelicate	-10806.6881671	77.9
$\Delta\Delta\Delta\Delta$ -Circular helicate	-10806.6988642	49.9
[2×2] grid	-10806.6994554	48.3
[Ti ₄ (L ²) ₄ (bipyraz) ₄]		
Alternate [2×2] grid	-10934.8577476	0.0
Cyclic hemihelicate	-10934.8159128	109.8
$\Delta\Delta\Delta\Delta$ -Circular helicate	-10934.8425891	39.8
[2×2] grid	-10934.8089084	128.2



 $[Ti_4(L^2)_4(bpym)_4]$ grid. Nevertheless, for the $[Ti_4(L^2)_4(bipyraz)_4]$ complex, the $\underline{C}H\cdots\underline{N}$ distances (mean $\underline{C}H\cdots\underline{N}$ distance=3.66 \pm 0.43 Å (Figure 8b)) are in average longer than those determined for the alternate $[2\times2]$ $[Ti_4(L^2)_4(bpym)_4]$ grid suggesting that the interactions are stronger for the $[Ti_4(L^2)_4(bpym)_4]$ complex (mean $\underline{C}H\cdots\underline{N}$ distance=3.33 \pm 0.25 Å (Figure 6b)).

Stability and selection studies

Having constructed the computed models of the tetranuclear circular species formed with the 2,2'-bipyrazine and the 2,2'bipyridine chelates, the stability of the alternate $[2\times2]$ [Ti₄(L²)₄(bpym)₄] grid towards the presence of these two diimine compounds was experimentally evaluated. The ligand exchange assays starting from the alternate $[2\times2]$ $[Ti_4(L^2)_4(bpym)_4]$ grid dissolved in CD2Cl2 were performed at 50°C with four equivalents of a given diimine compound. After 60 h, the mixture was analyzed by ¹H NMR revealing the presence of only the initial [Ti₄(L²)₄(bpym)₄] complex and the free bipyraz or bipy molecules and no further evolution of the composition of these mixtures was noticed overtime. This demonstrated the great thermodynamic stability of the alternate [2×2] grid formed with the bpym ligand. This was supported by the calculation of the thermodynamic parameters associated with the ligand exchange equations [Eq. (2) and (3)].

$$[Ti_4(L^2)_4(bpym)_4] + 4 bipy \Leftrightarrow [Ti_4(L^2)_4(bipy)_4] + 4 bpym$$
 (2)

$$\begin{aligned} & \left[\mathsf{Ti}_4(\mathsf{L}^2)_4(\mathsf{bpym})_4 \right] + 4 \ \mathsf{bipyraz} \\ & \leftrightharpoons \left[\mathsf{Ti}_4(\mathsf{L}^2)_4(\mathsf{bipyraz})_4 \right] + 4 \ \mathsf{bpym} \end{aligned} \tag{3}$$

Energy variations upon potential ligand exchange reactions using DFT (B3LYP // LANL2DZ) calculations were obtained for Equations (2) and (3). The modelled structures chosen for these calculations are the $[Ti_4(L^2)_4(bipyraz)_4]$, $[Ti_4(L^2)_4(bipy)_4]$ and $[Ti_4(L^2)_4(bpym)_4]$ alternate $[2\times2]$ grids. $\Delta E_{\rm reaction} =$ $\Sigma E_{\text{products}} - \Sigma E_{\text{reactants}}$ are found to be positive for both bipy or bipyraz pointing to the higher stability of the [Ti₄(L²)₄(bpym)₄] complex over the [Ti₄(L²)₄(bipy)₄] and [Ti₄(L²)₄(bipyraz)₄] complexes by 27.4 kcal/mol for the former and 30.2 kcal/mol for the latter and hence that no ligand exchange should be observed. Altogether, this theoretical approach indicates that the [Ti₄(L²)₄(bpym)₄] alternate grid is more stable comparatively to the computed alternate grids incorporating the bipyraz or bipy chelates. Thus, this prompted us to envision a selection study. [54] In other words, is it possible to selectively form the [Ti₄(L²)₄(bpym)₄] alternate grid when the pool of the initial compounds involved in the self-assembly process includes bipyraz and/or bipy in addition with the bpym chelate? In order to answer this question, the reactions were performed using the same reaction conditions as the one employed to generate [Ti₄(L²)₄(bpym)₄]. So, the mixtures containing the metal source, L²H₄ and the nitrogen ligands (bpym/bipy, bpym/bipyraz and bpym/bipy/bipyraz) in CDCl₃ were heated at 100°C under solvothermal conditions for 48 h. For all cases, an orange solid appeared in these media. These solids, as well as the remaining solutions were analysed by NMR and mass spectrometry. The ¹H NMR analysis of the solution, in each case, revealed only the presence of free diimine ligands with no trace of complexes were detected (see Supporting Information). The solids were analysed either by NMR or ES-MS depending on the solubility of the solid in CD₂Cl₂. Table 3 compiles the identified species that compose of the three isolated solids.

In parallel, the self-assembly reactions involving one single diimine ligand (bipy or bipyraz) were performed in CDCl $_3$ during one week at 100 °C. In this case, an orange solid was formed only with the bipy chelate. For the reaction conducted with bipyraz, the resulting orange solution was analyzed. The identified species found for these two reactions are given in Table 4.

This series of results are particularly informative. First, a tetranuclear aggregate [Ti₄(L²)₄(bipyraz)₄] was detected for the reaction conducted with the bipyraz ligand as confirmed by the NMR and ES-MS analysis of the reaction mixture. By mass spectrometry, a peak at m/z = 1595.90 corresponding to a tetranuclear assembly was detected (calcd for [Ti₄(L²)₄(bpym)₂+ 2H]²⁺: m/z=1595.39 (see Supporting Information)). The DOSY map (see Supporting Information) resulting from the analysis of the CDCl₃ solution revealed the presence of a large species diffusing at $D = 340 \,\mu\text{m}^2.\text{s}^{-1}$. From this diffusion, the hydrodynamic radius of $R_h = 11.9 \pm 10\%$ similar as the one obtained for [Ti₄(L²)₄(bpym)₄] was calculated. Also, the HSQC ¹H-¹⁵N experiment (see Supporting Information) permitted to assign 12 proton signals belonging to the bipyraz protons. Clearly, the complex obtained with bipyraz was an alternate [2×2] grid displaying the same C_2 -symmetry as $[Ti_4(L^2)_4(bpym)_4]$. The situation was different for the species incorporating bipy. Owing to the insolubility of the resulting solid, only the analysis by ES-MS was usable. Three intense peaks at high m/z were detected at m/z = 2623.71, m/z = 2467.61 and m/z = 2311.56corresponding to $[Ti_3(L^2)_3(bipy)_3 + H]^+$ (calcd m/z = 2623.70), $[Ti_3(L^2)_3(bipy)_2 + H]^+$ (calcd m/z = 2467.63) and $[Ti_3(L^2)_3(bipy) +$

Table 3. Composition of the solid isolated after the self-assembly process involving $Ti(O^iPr)_4$, L^2H_4 and bpym and one or two additional diimine ligands (bipy and bipyraz). ES-MS and 1H NMR spectra permitting the assignment of the species are given in Supporting Information.

bipyraz ^[a]	bipy ^[b]	bipyraz/bipy ^[b]
[Ti ₄ (L ²) ₄ (bpym) ₄]	$[Ti_2(L^2)_2(bipy)_4]$ $[Ti_4(L^2)_4(bipy)_4]$ $[Ti_3(L^2)_3(bipy)_3]$	$\begin{split} & [Ti_4(L^2)(L^2H)_3(bipy)_4(OH)_3] \\ & [Ti_3(L^2)_3(bipy)_3] \end{split}$
[a] Solid analyzed by ¹ H NMR. [b] Solid analyzed by ES-MS.		alyzed by ES-MS.

Table 4. Identified complexes after the self-assembly process involving $Ti(O^iPr)_4$, L^2H_4 and bipy or bipyraz. The reaction performed with bipy led to an orange solution, whereas for the reaction with bipy, an insoluble orange solid was isolated. ES-MS and 1H NMR spectra permitting the assignment of these species are given in Supporting Information.

	bipyraz ^[a]	bipy ^[b]
	[Ti ₄ (L ²) ₄ (bipyraz) ₄]	$[Ti_3(L^2)_3(bipy)_3]$
[a] Solution analyzed by ¹ H NMR and ES-MS. [b] Solid analyzed by ES-		i-MS. [b] Solid analyzed by ES-MS.



H]⁺ (calcd m/z = 2311.56) respectively demonstrating the formation of a trinuclear assembly. Next, these results gained form the reaction performed with one ligand were compared with those obtained in the course of the competition study. For the process involving the bpym/bipyraz combination, only the alternate $[2\times2]$ $[Ti_4(L^2)_4(bpym)_4]$ grid was characterized for the solid and the solution contains a large majority of bipyraz vs. bpym (bipyraz /bpym ratio = 2.6). Clearly, this indicates that a selection occurred in the course of the self-assembly process. For the experiment conducted with bpym/bipy, the situation was more complex since several products composed the analyzed solid. ES-MS analysis highlighted the presence of di-, tri- and tetranuclear aggregates with no trace of an assembly containing the bpym ligand. An identical observation was made for the reaction performed with the three diimine compounds, for example bpym/bipy/bipyraz since only species incorporating the bipy chelate were detected (Table 3). This concerns a tetranuclear assembly formulated as [Ti₄(L²)(L²H)₃(OH)₃(bipy)₄] where several titanium atoms are coordinated by a hydroxo ligand and a trinuclear assembly formulated as [Ti₃(L²)₃(bipy)₃]. Altogether, this competition study, for which the results are summarized in Figure 9, permits to extract fundamental information related the factors regulating the self-assembly processes within these systems. First, it is possible to discriminate two closely related diimine ligands, bpym and bipyraz, in the course of the self-assembly process and to select only the alternate $[2\times2]$ $[Ti_4(L^2)_4(bpym)_4]$ grid. All the reactions conducted with bipy end to the formation of [Ti₃(L²)₃(bipy)₃]. This stresses the fact that, in the absence of N···HC interactions, the natural evolution of the system goes to the generation of the trinuclear assembly and consequently that N···HC interactions are essential to stabilize tetranuclear architectures. Meanwhile, aggregates built from bipy possessing other nuclearities are also spotted with, in particular, an assembly where the Ti-OH linkage is found. This highlights some intermediates of the selfassembly reaction pathway conducting to [Ti₃(L²)₃(bipy)₃] and suggests that the conversion of these intermediates into the final trinuclear species passes through the formation of Ti-OH linkages.

Conclusion

Herein, we have reported a self-assembly reaction conducted with $Ti(O^iPr_4)$, the 2,2'-bipyrimidine ligand and a bis-2,2'-biphenol strand. We have shown that the incorporation of a

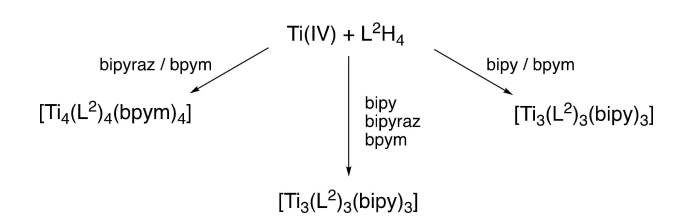


Figure 9. Main species characterized in the course of the competition studies.

biphenyl spacer within the strand permitted to generate the stable tetranuclear [Ti₄(L²)₄(bpym)₄] architecture. This investigation proved that the nature of the spacer is an essential factor, in addition to the structure of the diimine chelate, to govern the nuclearity of the self-assembled architectures based on TiO₄N₂ motifs. The solid-state structure of [Ti₄(L²)₄(bpym)₄] indicated the formation of an unprecedented chiral alternate [2×2] grid where the intramolecular CH···N interactions resulting from the closed disposition of two bpym ligands explain the formation of this original structure. Undoubtedly, these weak CH···N interactions permit to stabilize the tetranuclear assembly since [Ti₄(L²)₄(bipyraz)₄] is formed and its modelled structure also revealed the same kind of interactions. Furthermore, this point is strongly supported by the formation of a trinuclear species with the bipy ligand for which no CH···N interaction could occur. Finally, a competition between two ligands, bpym and bipyraz, has been conducted and leads exclusively to the $[Ti_4(L^2)_4(bpym)_4]$ formation. As far as we aware, this is the first example where a grid-type structure is able to select one precise diimine ligand in the course of a selfassembly process.

Experimental Section

All the following reactions were conducted under argon atmosphere, unless mentioned otherwise. Polar solvents were dried using a 3 Å molecular sieve and apolar solvents, a 4 Å molecular sieve. A drying time of at least five hours is respected before use of dried solvents. Bruker Avance-300, Avance-400, Avance-500 and Avance 600 were used for solution NMR analysis. ¹H NMR DOSY measurements were performed at 600 MHz. The range of temperatures for dynamic NMR were met using a refrigerating and heating system and measurements were acquired at 400 MHz and 600 MHz. Data analysis and curve fitting for the latter experiment was enabled using TopSpin Academia v3.5. The Electrospray analyses were performed on a MicroTOF (Bruker) apparatus equipped with an electrospray (ES) source. The solids were dissolved in CH₂Cl₂ or CHCl₃ according to their solubility and the resulting solutions were analyzed.

2',2"',2""",2"""Tetramethoxy-

1,1':3',1"':3",1"':4"',1"":4"",1""":3""",1""":3""",1"""-octophenyl, L²Me₄: The Suzuki-Miyaura coupling reaction was conducted under argon. In 100 mL two-neck round-bottom flask, Na₂CO₃ (2 M, 10 mL) and tetrahydrofuran (10 mL) were added to degassed 4,4'-dibromophenyl (0.237 g, 7.60×10⁻⁴ mol) and (2,2'-dimethoxy-[1,1':3",1"terphenyl]-3-yl)boronic acid (0.5 g, 1.52×10^{-3} mol). The reaction was then catalyzed by $Pd(PPh_3)_4$ (0.176 g, $1.52\times 10^{-4}\, mol).$ The system was then heated to reflux and stirred overnight. The completion of reaction was confirmed by TLC (*n*-pentane/CH₂Cl₂, 70:30). After cooling, the reaction mixture was washed twice with distilled H₂O (100 mL), subsequently dried with Na₂SO₄, and concentrated under reduced pressure. Product was purified via silica gel chromatography ($\emptyset = 3.2$ cm, I = 25 cm; CH₂Cl₂) to afford a white solid (0.372 g, 67%). M.p. 200 $^{\circ}$ C. 1 H NMR (500 MHz, CDCl $_{3}$): δ = 7.72 (s, 8 H), 7.62 (m, 4 H), 7.49-7.31 (complex, 14 H), 7.28-7.18 (complex, 4 H), 3.31 (s, 6 H, OMe), 3.27 (s, 6 H, OMe) ppm. ¹³C NMR (125 MHz, CDCl₃) δ = 155.5, 155.3, 139.4, 138.9, 137.9, 135.1, 134.6, 133.0, 132.9, 131.0, 130.9, 130.6, 130.5, 129.7, 129.2, 128.2, 127.1, 126.8, 123.7, 123.6, 60.7, 60.6 ppm. MS: (ES) calcd. for [M+K]+770.002, found 769.27. Elemental analysis: C52H42O4 calcd. C 85.50, H 5.80; found C 85.00, H 5.77.



2',2",2"''',2"'''Tetrahydrox-y-1,1':3',1"':3",1"':4"',1"'':4"'',1"''':3"''',1"'':3"''',1"''''-octophenyl, L^2H_4 :

The reaction was conducted under argon. Compound L²Me₄ (0.29 g, 3.98×10^{-4} mol) was dissolved in anhydrous CH₂Cl₂ (20 mL). The system was cooled to -78 °C, and then BBr₃ (1 M in CH₂Cl₂, 1.75 mL, 1.75×10^{-3} mol) was added to the solution. The reaction mixture was allowed to warm to room temperature and stirred overnight. The reaction mixture was cooled to 0°C, and the remaining BBr₃ was hydrolyzed via the dropwise addition of distilled water. Additional anhydrous CH₂Cl₂ (200 mL) was added to dissolve the product. The organic mixture was washed with distilled water (150 mL), dried over Na₂SO₄, and concentrated under reduced pressure to afford a yellow solid (0.241 g, 90%). M.p. 237 °C. ¹H NMR (500 MHz, CDCl₃): $\delta = 7.75$ (d, 4 H, $^{3}J = 8.3$ Hz), 7.68 (d, 4H, $^{3}J =$ 8.3 Hz), 7.57 (d, 4H, ${}^{3}J=7.1$ Hz), 7.47 (t, 4H, ${}^{3}J=7.5$ Hz), 7.43-7.32 (complex, 10 H), 7.18-7.10 (complex, 4H), 5.90 (bs, 2 H, OH), 5.81 (bs 2 H, OH) ppm. 13 C NMR (CDCl₃, 125 MHz) δ = 149.9, 149.6,139.9, 137.3, 136.7, 131.2, 131.1, 130.8, 130.7, 129.9, 129.5, 129.4, 129.2, 128.9, 127.8, 127.4, 125.1, 127.7, 121.5, 121.5 ppm MS: (ES) calcd. for [M]+ 675.68, found 675.25. Elemental analysis: C48H34O4.4THF (analyzed sample was obtained by crystallization in tetrahydrofuran solution) calcd. C 79.83 %, H 6.86 %; found C 79.95 %, H 6.61 %.

 $[Ti_4(L^2)_4(bpym)_4]$: A vial with the dry ligands L^2H_4 (20 mg, 2.96× 10^{-5} mol) and 2,2'-bipyrimidine (4.7 mg, 2.96×10^{-5} mol) was placed under argon. The ligands then were dissolved in 1.5 mL of dry chloroform. Via microsyringe, [Ti(OⁱPr)₄] (7.4 µL, 2.96×10⁻⁵ mol) was added and created a dark orange solution. The sealed vial was put in a 100 °C dry bath where red crystals began to form over the next week. By pipetting the orange solution of impurities and unreacted material, the red crystals were isolated (21.0 mg, 81% yield). ¹H NMR (500 MHz, CD $_2$ CI $_2$): $\delta\!=\!9.88$ (dd, J=4.9, 2.2 Hz, 2 H), 8.95 (dd, J=4.9, 2.4 Hz, 2 H), 8.84 (dd, J=5.4, 2.3 Hz, 2 H), 8.74 (dd, J=5.5, 2.3 Hz, 2 H), 8.33 (dd, J = 5.3, 2.3 Hz, 2 H), 8.26 (dd, J = 5.6, 2.2 Hz, 2 H), 7.95 (dd, J=4.9, 2.5 Hz, 2 H), 7.93 (dd, J=4.7, 2.2 Hz, 2 H), 7.55 (d, J=8.3 Hz, 4 H), 7.46-6.78 (complex, 65 H), 6.74 (t, J=7.7 Hz, 4 H), 6.69 (t, J = 5.1 Hz, 4 H), 6.65 (dd, J = 7.8, 2.0 Hz, 4 H), 6.56 (t, J =7.6 Hz, 4 H), 6.48 (dd, J=7.4, 1.6 Hz, 4 H) ppm. ¹³C NMR (125 MHz, CD_2CI_2) $\delta = 165.4$, 162.7, 161.0, 160.3, 160.2, 160.1, 160.0, 159.5, 159.4, 159.3, 158.9, 158.0, 158.6, 158.1, 156.3, 155.8, 155.4, 154.6, 138.9, 138.6, 138.4, 138.3, 138.3, 137.8, 137.4, 136.6, 136.6, 136.4, 135.8, 132.3, 132.0, 131.6, 131.1, 130.8, 130.5, 130.2, 129.9, 129.7, 129.6, 129.6, 129.5, 129.4, 129.4, 129.3, 129.2, 129.1, 129.0, 128.8, 128.5, 128.0, 127.6, 127.5, 127.3, 127.0, 126.4, 126.3, 125.9, 125.7, 125.5, 122.5, 122.4, 122.1, 121.7, 121.6, 120.7, 120.1, 119.9, 119.6 ppm. MS: (ES) calcd. for $[M+2H]^{2+}$ 1753.45, found 1753.44. Elemental analysis [Ti₄(L²)₄(bpym)₄]. 6 CHCl₃ calcd. C 65.41%, H 3.58%, N 5.31%; found C 65.06%, H 4.02%, N 6.18%,

X-ray diffraction data

Single crystal X-ray diffraction data for the [Ti₄(L²)₄(bpym)₄] compound were collected with a RigakuFRX rotating anode (2.97 kW) diffractometer at the IECB x-ray facility (CNRS UMS 3033 – INSERM US001, Université de Bordeaux). CuKα radiation monochromated with high flux Osmic Varimax mirrors was used for data collection. The x-ray source is equipped with a Dectris Pilatus 200 K detector and an AFC11 partial chi goniometer allowing omega scans. The crystal was mounted on a cryoloop and flash-frozen under a nitrogen gas stream at 130(2) K. Data were processed with the CrysAlis PRO^[55] software. The structure was solved with the ShelXT^[56] structure solution program using Intrinsic Phasing. The Olex2 suite^[57] was used for model building and structure refinement with the ShelXL^[58] package running Least Squares minimization. H atoms were positioned geometrically and constrained

depending on their environment. Those H-atoms were refined in the riding-model approximation, with Uiso(H) = 1.2 Ueq (CH, CH2, NH). RESI, DFIX, AFIX, and RIGU restraints were apply to model geometry of the molecules and thermal motion parameters. Deposition Number 2005272 (for $3[\mathrm{Ti}_4(\mathrm{L}^2)_4(\mathrm{bpym})_4])$ contains the supplementary crystallographic data for this paper. These data are provided free of charge by the joint Cambridge Crystallographic Data Centre and Fachinformationszentrum Karlsruhe Access Structures service.

Empirical formula: $C_{667}H_{434}Cl_{21}N_{48}O_{51}Ti_{12}$, Formula weight 11255.54, Temperature/K 130.0, Crystal system orthorhombic, Space group Fdd2, a/Å 50.5331(8), b/Å 121.3748(15), c/Å 41.8102(8), α/° 90 β/° 90 γ/° 90, Volume/ 256441(7) Å3, Z=16, ρ_{calc} g/cm³, 1.166 μ/mm⁻¹ 2.532. F(000) 92816.0, Crystal size/mm³ 0.01×0.01×0.01, Radiation CuKα (λ =1.54178), Reflections collected 309871, Independent reflections 78388 [R_{int}=0.0869, R_{sigma}=0.0605]. Data/restraints/ parameters 78388/65419/6881, Goodness-of-fit on F2 1.207, Final R indexes [I > =2σ (I)], R1=0.1074, wR2=0.2987, Final R indexes [all data], R1=0.1349, wR2=0.3334, Largest diff. peak/hole/e Å⁻³0.71/=0.46.

DFT calculations

DFT calculations were performed using the GAUSSIAN 09software. $^{[59]}$

Energies of bipy, bipyraz and bpym used to calculate $\Delta E_{\rm reaction}$ associated to the reactions Equation (2) and Equation (3) are in Hartree: E(bpym) = -527.341568741, E(bipy) = -495.308567933; E-(bipyraz) = -527.344671906.

Acknowledgements

We thank the National Science Foundation, CHE-1659782, funded Research Experience for Undergraduates exchange program with University of Florida (ED). We are grateful to the University of Strasbourg and the CNRS for financial support. M. Scarpi-Luttenauer thanks the French Ministry of Research for his PhD fellowship.

Conflict of Interest

The authors declare no conflict of interest.

Data Availability Statement

The data that support the findings of this study are available from the corresponding author upon reasonable request.

Keywords: alternate grid \cdot CH···N interactions \cdot selection \cdot DFT calculations \cdot TiO₄N₂

- [1] J.-M. Lehn, Supramolecular Chemistry Concepts and Perspectives, Weinheim, 1995.
- [2] A. J. McConnell, C. S. Wood, P. P. Neelakandan, J. R. Nitschke, Chem. Rev. 2015, 115, 7729–7793.
- [3] M. Albrecht, Chem. Rev. 2001, 101, 3457–3497.



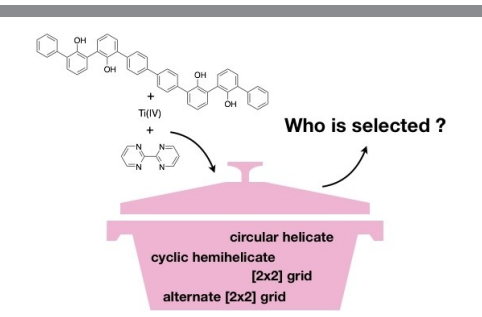
- [4] C. Piguet, G. Bernardinelli, G. Hopfgartner, Chem. Rev. 1997, 97, 2005– 2062
- [5] G. Gil-Ramírez, D. A. Leigh, A. J. Stephens, Angew. Chem. Int. Ed. 2015, 54, 6110–6150; Angew. Chem. 2015, 127, 6208–6249.
- [6] J. F. Ayme, J. E. Beves, C. J. Campbell, D. A. Leigh, Chem. Soc. Rev. 2013, 42, 1700–1712.
- [7] W. X. Gao, H. J. Feng, B. B. Guo, Y. Lu, G. X. Jin, Chem. Rev. 2020, 120, 6288–6325.
- [8] S. J. Lee, J. T. Hupp, Coord. Chem. Rev. 2006, 250, 1710-1723.
- [9] D. Fujita, Y. Ueda, S. Sato, H. Yokoyama, N. Mizuno, T. Kumasaka, M. Fujita, Chem 2016, 1, 91–101.
- [10] T. R. Cook, P. J. Stang, Chem. Rev. 2015, 115, 7001-7045.
- [11] P. Jin, S. J. Dalgarno, J. L. Atwood, Coord. Chem. Rev. 2010, 254, 1760– 1768.
- [12] M. Fujita, M. Tominaga, A. Hori, B. Therrien, Acc. Chem. Res. 2005, 38, 369–378.
- [13] D. L. Caulder, K. N. Raymond, Acc. Chem. Res. 1999, 32, 975-982.
- [14] M. Ruben, J. Rojo, F. J. Romero-Salguero, L. H. Uppadine, J. M. Lehn, Angew. Chem. Int. Ed. 2004, 43, 3644–3662; Angew. Chem. 2004, 116, 3728–3747.
- [15] A. M. Stadler, Eur. J. Inorg. Chem. 2009, 32, 4751–4770.
- [16] L. N. Dawe, K. V. Shuvaev, L. K. Thompson, Chem. Soc. Rev. 2009, 38, 2334–2359.
- [17] J. G. Hardy, Chem. Soc. Rev. 2013, 42, 7881-7899.
- [18] M. A. Naumova, A. Kalinko, J. W. L. Wong, M. Abdellah, H. Geng, E. Domenichini, J. Meng, S. A. Gutierrez, P. A. Mante, W. Lin, et al., J. Phys. Chem. Lett. 2020, 11, 2133–2141.
- [19] M. A. Rosero-Mafla, J. I. Castro, N. E. Sánchez, C. A. Mujica-Martinez, M. N. Chaur, ChemistrySelect 2020, 5, 7685–7694.
- [20] Y. T. Wang, S. T. Li, S. Q. Wu, A. L. Cui, D. Z. Shen, H. Z. Kou, J. Am. Chem. Soc. 2013, 135, 5942–5945.
- [21] S. Q. Wu, Y. T. Wang, A. L. Cui, H. Z. Kou, *Inorg. Chem.* 2014, 53, 2613–2618.
- [22] M. A. Gordillo, M. Soto-Monsalve, C. C. Carmona-Vargas, G. Gutiérrez, R. F. D'vries, J. M. Lehn, M. N. Chaur, Chem. Eur. J. 2017, 23, 14872– 14887
- [23] J. W. L. Wong, S. Demeshko, S. Dechert, F. Meyer, *Inorg. Chem.* 2019, 58, 13337–13345.
- [24] M. Steinert, B. Schneider, S. Dechert, S. Demeshko, F. Meyer, *Inorg. Chem.* 2016, 55, 2363–2373.
- [25] W. Huang, F. X. Shen, S. Q. Wu, L. Liu, D. Wu, Z. Zheng, J. Xu, M. Zhang, X. C. Huang, J. Jiang, et al., *Inorg. Chem.* 2016, 55, 5476–5484.
- [26] P. N. W. Baxter, J. M. Lehn, B. O. Kneisel, D. Fenske, Chem. Commun. 1997, 22, 2231–2232.
- [27] B. M.-T. Youinou, N. Rahmouni, J. Fisclwr, J. A. Osborn, *Angew. Chem. Int. Ed. Engl.* 1992, 31, 733–735.
- [28] T. Bark, M. Düggeli, H. Stoeckli-Evans, A. von Zelewsky, Angew. Chem. Int. Ed. Engl. 2001, 40, 2848–2851.
- [29] P. Baxter, J.-M. Lehn, G. Baum, D. Fenske, Chemistry (Easton). 2000, 6, 4510–4517.
- [30] M. Barboiu, F. Dumitru, E. Petit, Y. M. Legrand, A. V. D. Lee, Supramol. Chem. 2015, 27, 393–400.
- [31] E. C. Constable, *Chem. Soc. Rev.* **2013**, *42*, 1637–1651.
- [32] M. Barboiu, E. Petit, A. Van Der Lee, G. Vaughan, *Inorg. Chem.* 2006, 45, 484–486.
- [33] M. L. N. Rao, H. Houjou, K. Hiratani, Chem. Commun. 2002, 918, 420-421.
- [34] T. Kreickmann, C. Diedrich, T. Pape, H. V. Huynh, S. Grimme, F. E. Hahn, J. Am. Chem. Soc. **2006**, *128*, 11808–11819.
- [35] M. Albrecht, S. Kotila, Angew. Chem. Int. Ed. Engl. 1995, 34, 2134–2137.

- [36] X. Chen, T. M. Gerger, C. Räuber, G. Raabe, C. Göb, I. M. Oppel, M. Albrecht, Angew. Chem. Int. Ed. Engl. 2018, 57, 11817–11820.
- [37] N. Ousaka, M. Itakura, A. Nagasaka, M. Ito, T. Hattori, D. Taura, T. Ikai, E. Yashima, J. Am. Chem. Soc. 2021, 11, 4346–4358.
- [38] E. J. Corey, C. L. Cywin, M. C. Noe, Tetrahedron Lett. 1994, 35, 69-72.
- [39] R. Fandos, C. Hernández, A. Otero, J. Pacheco, A. M. Rodríguez, M. J. Ruiz, J. Á. Organero, Organometallics 2018, 37, 3515–3523.
- [40] Y. P. He, L. B. Yuan, J. S. Song, G. H. Chen, Q. Lin, C. Li, L. Zhang, J. Zhang, Chem. Mater. 2018, 30, 7769–7775.
- [41] B. C. Zhu, W. H. Fang, J. Wang, Y. Du, T. Zhou, K. Wu, L. Zhang, J. Zhang, Chem. Eur. J. 2018, 24, 14358–14362.
- [42] C. Diebold, D. M. Weekes, M. Torres Navarrete, P. Mobian, N. Kyritsakas, M. Henry, Eur. J. Org. Chem. 2010, 36, 6949–6956.
- [43] G. Khalil, L. Barloy, N. Kyritsakas, P. Mobian, M. Henry, *Dalton Trans*. 2018, 47, 11113–11122.
- [44] N. Baradel, P. Mobian, G. Khalil, M. Henry, *Dalton Trans.* **2017**, *46*, 7594–
- [45] E. Macker, L. Barloy, A. Chaumont, N. Kyritsakas, B. Vincent, M. Henry, P. Mobian, Inorg. Chim. Acta 2019, 498, 119119.
- [46] P. Mobian, N. Baradel, N. Kyritsakas, G. Khalil, M. Henry, Chem. Eur. J. 2015, 21, 2435–2441.
- [47] G. Khalil, L. Barloy, N. Kyritsakas, B. Kauffmann, A. Chaumont, M. Henry, P. Mobian, Eur. J. Inorg. Chem. 2020, 36, 3527–3531.
- [48] J. F. Ayme, J. M. Lehn, C. Bailly, L. Karmazin, J. Am. Chem. Soc. 2020, 142, 5819–5824.
- [49] P. J. Dunning, T. H. Jr. Hay, In: H. F. Schaefer III, Ed., Methods of Electronic Structure Theory, Vol. 2, Plenum, New York, 1977.
- [50] P. J. Hay, W. R. Wadt, J. Chem. Phys. 1985, 82, 270-283.
- [51] W. R. Wadt, P. J. Hay, J. Chem. Phys. 1985, 82, 284-298.
- [52] S. Grimme, J. Antony, S. Ehrlich, H. Krieg, J. Chem. Phys. 2010, 132, 154104.
- [53] J.-D. Chai, M. Head-Gordon, Phys. Chem. Chem. Phys. 2008, 10, 6615–6620.
- [54] J. M. Lehn, Eur. Rev. 2009, 17, 263-280.
- [55] Rigaku Oxford Diffraction (2015). CrysAlis PRO. RigakuOxford Diffraction, Yarnton, England.
- [56] G. M. Sheldrick, Acta Crystallogr. 2015, A71, 3-8.
- [57] O. V. Dolomanov, L. J. Bourhis, R. J. Gildea, J. A. K. Howard, H. Pusch-mann, J. Appl. Crystallogr. 2009, 42, 339–341.
- [58] G. M. Sheldrick, Acta Crystallogr. 2015, C71, 3-8.
- [59] M. J. Frisch, G. W. Trucks, H. B. Schlegel, G. E. Scuseria, M. A. Robb, J. R. Cheeseman, G. Scalmani, V. Barone, B. Mennucci, G. A. Petersson, H. Nakatsuji, M. Caricato, X. Li, H. P. Hratchian, A. F. Izmaylov, J. Bloino, G. Zheng, J. L. Sonnenberg, M. Hada, M. Ehara, K. Toyota, R. Fukuda, J. Hasegawa, M. Ishida, T. Nakajima, Y. Honda, O. Kitao, H. Nakai, T. Vreven, J. A. Jr. Montgomery, J. E. Peralta, F. Ogliaro, M. Bearpark, J. J. Heyd, E. Brothers, K. N. Kudin, V. N. Staroverov, T. Keith, R. Kobayashi, J. Normand, K. Raghavachari, A. Rendell, J. C. Burant, S. S. Iyengar, J. Tomasi, M. Cossi, N. Rega, J. M. Millam, M. Klene, J. E. Knox, J. B. Cross, V. Bakken, C. Adamo, J. Jaramillo, R. Gomperts, R. E. Stratmann, O. Yazyev, A. J. Austin, R. Cammi, C. Pomelli, J. W. Ochterski, R. L. Martin, K. Morokuma, V. G. Zakrzewski, G. A. Voth, P. Salvador, J. J. Dannenberg, S. Dapprich, A. D. Daniels, O. Farkas, J. Foresman, J. V. Bortiz, J. Cioslowski, D. J. Fox, Gaussian 09 (Rev. D.01); Gaussian, Inc.: Wallingford, CT, 2013.

Manuscript received: January 7, 2022
Accepted manuscript online: February 8, 2022
Version of record online:

RESEARCH ARTICLE

The synthesis of an alternate $[2 \times 2]$ grid constructed around four TiO₄N₂ units is described. This chiral architecture is generated from the 2,2-bipyrimidine ligand and a tetraphenolic strand. The formation of this tetranuclear assembly is driven by CH···N interactions. In the course of the selfassembly process, the system is able to select one diimine ligand in the pool of the initial components.



E. Day, B. Kauffmann, M. Scarpi-Luttenauer, A. Chaumont, M. Henry, P. Mobian*

1 – 10

An Alternate [2×2] Grid Constructed Around TiO₄N₂ Units

